Robotica (2012) volume 30, pp. 1213–1219. © Cambridge University Press 2012
doi:10.1017/S0263574712000045

Optimization design for a jumping leg robot based on generalized inertia ellipsoid

Jianjun Yao†*, Qi Yang‡, Shuang Gao† and Shenghai Hu†

†*College of Mechanical and Electrical Engineering, Harbin Engineering University, Harbin 150001, China*
‡*Institute of Structural Mechanics, CAEP, Mianyang 621900, China*

(Accepted January 31, 2012. First published online: February 27, 2012)

SUMMARY
The isotropy of the generalized inertia ellipsoid is an evaluation index that can measure dynamic performance of a robot. This has significance in motion planning and design of a jumping robot. The generalized inertia of a jumping robot is analyzed. The generalized inertia tensor and the generalized inertia ellipsoid (GIE) are derived from the kinetic energy of the robot mechanism. From the viewpoint of geometrical shape change of the GIE, nonlinear characteristics of a jumping robot are analyzed. With the goal of minimizing nonlinear effects during its movement, the mechanism parameters of a jumping robot are optimized by adopting isotropy of the generalized inertia ellipsoid as its objective function. Example results demonstrate the efficiency and validity of the proposed optimization method.

KEYWORDS: Jumping robot; Generalized inertia tensor; Generalized inertia ellipsoid; Nonlinear characteristics; Isotropic condition; Optimization design.

1. Introduction

Jumping is an important motion for many biological creatures, such as locusts, springtails, kangaroo and fleas. This motion style has clear advantages in terms of the terrain adaptability and energy efficiency.[1] It is a very efficient locomotion for robots to overcome large obstacles and to travel in natural rough terrain. For a robot with jumping gait, its motion range can be greatly extended. Jumping robots, which can store energy by compressing an elastic mechanism that could quickly release the energy during jumping process, have good application prospect because these can move over rough terrains with uneven surfaces, jump over obstacles and ditches.[2,3] These properties make them suitable for operation in the human environment and dangerous applications,[4] such as archaeology survey, space exploration, military reconnaissance, geological prospecting, forest protection, emergency rescue and disaster relief and anti-terrorist rescue. Such advantages have inspired robotic scientists and engineers to investigate and develop jumping robots by mimicking biological jumping principles of different jumping creatures.[5]

The development of a jumping robot can be dated from hopping robot with simple structure to complex bionic jumping robot. Currently, miniaturization, intelligence and application of biological principles are the development trends of jumping robots. Yamakita *et al.*[6] studied a jumping cat robot moving in a vertical direction by mimicking cat behavior. Arikawa and Mita[7] designed a multi-degrees of freedom (DOF) jumping robot composed of five links and four joints that was serial linked and discussed the process to determine the design parameters, including mechanical parameters and motion planning parameters from the view point of realizing actual mechanical model. Hyon *et al.*[8] developed a gymnastic robot, which was a planar and serially connected four-link robot for various floor exercises, such as jumping, somersault and back handspring. Based on the kinematics of a cricket, researchers of Case Western Reserve University, Cleveland, OH, developed an autonomous robot that was actuated by braided pneumatic actuators with compressed air provided by an onboard compressor and distributed by an array of actuated micro-electromechanical systems (MEMS) valves.[9,10] Using imitation of a running dog, Hyon and Mita[11] proposed a simple mechanical model for hind limb of a dog to realize a robot with an articulated leg, as well as the hardware design of one-legged running robot, and used two hydraulic actuators as muscles and a tensile spring as a tendon, enabling the robot to produce sufficient propulsion force by virtue of energy transfer from knee, even if there was no actuator at the ankle joint. Niiyama *et al.*[12] investigated a pneumatically actuated bipedal robot with artificial musculoskeletal system, which comprised six McKibben pneumatic muscle actuators, including bi-articular muscle and two legs with hip, knee and ankle joints, reaching jump heights of more than 50% of its body height and can land softly. Wong and Orin[13] studied a quadruped standing jump that could jump over irregular terrain obstacles, and planned simple open-loop leg forces to remove the large linear and angular momentum of the body during landing. Yang *et al.*[14] proposed a type of planar one legged robot with three revolute joints, two links and two feet, and designed a cyclic flipping gait. He *et al.*[15] investigated an elastic one-legged hopping robot, which was constructed by two actuated arms and an elastic passive telescopic leg, and developed motion control algorithm for hopping control in vertical direction based on nonlinear transformation of inputs for this kind of under-actuated non-holonomic dynamic system. Ma *et al.*[16] studied a kangaroo hopping robot and analyzed its structure, gaits and motion characteristics.

* Corresponding author. E-mail: travisyao@126.com

https://doi.org/10.1017/S0263574712000045 Published online by Cambridge University Press

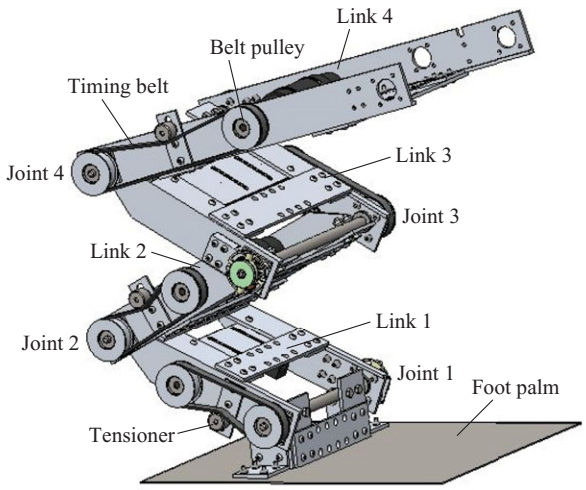


Fig. 1. (Colour online) The jumping leg robot.

The current research on jumping robots is mainly focused on robot structure, dynamic characteristics, control system and so forth. However, designing a jumping robot is not a simple process because of the highly nonlinear and coupled dynamics of the structure. What is more, the design parameters have great influence on the kinematic and dynamic characteristics of a jumping robot. Optimization technique is applied here to determine the design parameters to represent the jumping robot and its dynamics so that these could be easily understood by the designer and the jumping robot's dynamics could be improved.

Asada[17] provided a geometrical interpretation, generalized inertia ellipsoid (GIE), to describe the dynamics of robot arm. He extended the inertia ellipsoid of a single rigid body to a series of rigid bodies to analyze the dynamics of robot arm, determining the robot workspace. Using the Eigenvalues of Cartesian inertia vector, GIE can measure the acceleration characteristics of a manipulator along the Cartesian direction. The dynamic performance can be analyzed from the GIE configuration, from which the complex inertia effects and the nonlinear coupling characteristics of multi-DOF motion can also be understood.

Here, the jumping robot in the ground phase, including take-off and landing, can be considered as a manipulator. The concept of GIE used in mechanical arm can then be applied to the optimization of mechanism parameters of the jumping robot to improve robot's dynamic performance.

2. Generalized Inertia Analysis of a Jumping Robot

2.1. Generalized inertia tensor

Figure 1 shows the jumping leg robot, which is made of aluminum alloy material. It comprises four joints driven by DC servomotors and four links with timing belt transmission composed of timing belt, belt pulley and tensioner. The state of the ground phase of the jumping robot in Fig. 1 is shown in Fig. 2 with simplified mechanism model.

During the state of the ground phase, the robot can be regarded as a four-link serial manipulator with redundant DOF. For a single rigid body, its motion can be decomposed

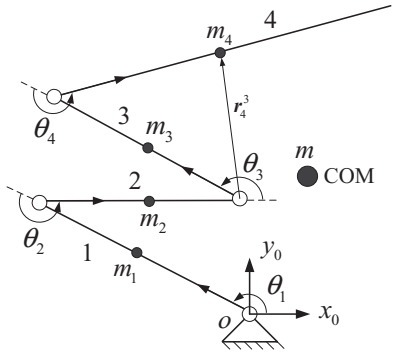


Fig. 2. The mechanism model in the ground phase.

into a translation with respect to its center of mass (COM) and a rotation about the center. Let v_i be the translational velocity and ω_i be the angular velocity. Thus, the kinetic energy of link i is

$$E_{ki} = \frac{1}{2} m_i v_i^T v_i + \frac{1}{2} \omega_i^T I_i \omega_i, \tag{1}$$

where m_i is the mass of ith link, and I_i is the inertia tensor. The motion of each link is constrained by linkage. Let θ_i be the displacement of joint i, and its time derivative is $\dot{\theta}_i$. Thus, the velocity of link i can be expressed by

$$\boldsymbol{\omega}_i = \sum_{j=1}^{i} \boldsymbol{a}_j \dot{\theta}_j, \ \boldsymbol{v}_i = \sum_{j=1}^{i} \boldsymbol{b}_j \dot{\theta}_j, \tag{2}$$

where $\boldsymbol{a}_j$ is a unit vector pointing in the direction of the ith joint axis, and $\boldsymbol{b}_j$ is the vector product between the position vectors $\boldsymbol{r}_i^j$ and $\boldsymbol{a}_j$, that is $\boldsymbol{b}_j = \boldsymbol{a}_j \times \boldsymbol{r}_i^j$. Substituting Eq. (2) into Eq. (1), the total kinetic energy of the jumping robot is[18]

$$E_k = \frac{1}{2} \dot{\boldsymbol{\theta}}^T \boldsymbol{M} \dot{\boldsymbol{\theta}}, \tag{3}$$

where $\dot{\boldsymbol{\theta}} = [\dot{\theta}_1, \cdots, \dot{\theta}_4]^T \in R^{4\times 1}$ and $\boldsymbol{M} = \sum_{i=1}^{4} (A_i^T I_i A_i + m_i B_i^T B_i) \in R^{4\times 4}$, in which $\boldsymbol{A}_i = [a_1, \ldots, a_i, 0, \ldots, 0]$ and $\boldsymbol{B}_i = [b_1, \ldots, b_i, 0, \ldots, 0]$, is a symmetric matrix.

The kinetic energy can also be expressed in the Cartesian operation space. The motion of the jumping robot in the operation space is planar motion. Selecting the generalized coordinates of the whole COM of the robot as $\boldsymbol{x} = [x_1, x_2]$, the kinetic energy expressed in the Cartesian operation space is

$$E_k = \frac{1}{2} \dot{\boldsymbol{x}}^{\mathrm{T}} \boldsymbol{G} \dot{\boldsymbol{x}}, \tag{4}$$

where $\boldsymbol{G} = \boldsymbol{J}^{-\mathrm{T}} \boldsymbol{M} \boldsymbol{J}^{-1}$, in which $\boldsymbol{J}$ is the Jacobian matrix. The symmetric matrix, $\boldsymbol{G}$, is called the generalized inertia tensor.[17]

2.2. Generalized Inertia Ellipsoid (GIE)

For the generalized inertia tensor, $\boldsymbol{G}$, its quadratic form is

$$\mathbf{u}^T \boldsymbol{G} \mathbf{u} = \mathbf{I}. \tag{5}$$

https://doi.org/10.1017/S0263574712000045 Published online by Cambridge University Press

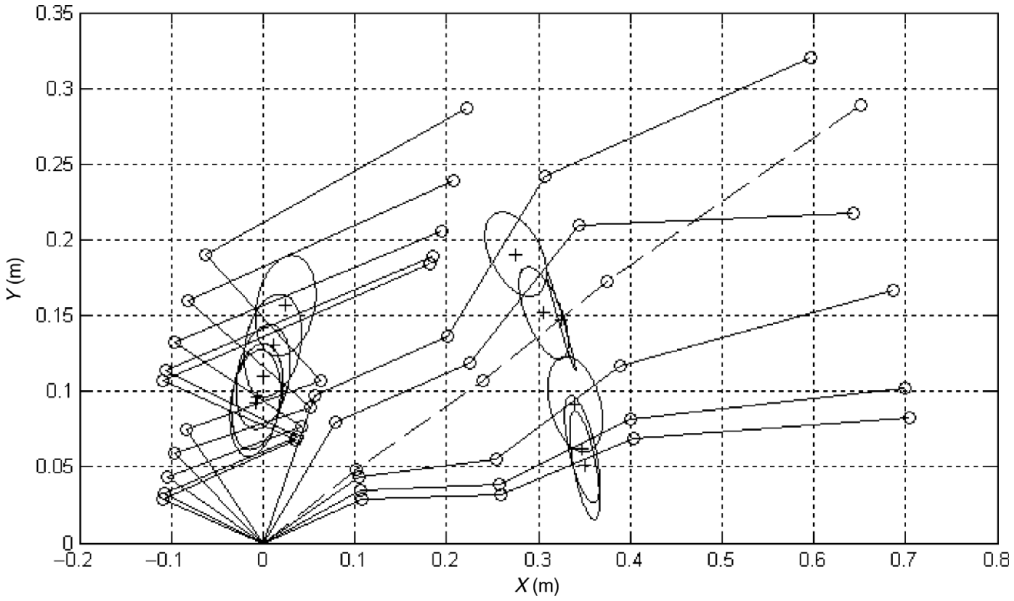


Fig. 3. GIE of the jumping leg robot.

It is a quadratic surface. The symmetric matrix is positive definite because the kinetic energy, E_k, is always positive except when $\dot{\boldsymbol{x}} = 0$. Equation (5) denotes an ellipsoid in the space. For a single rigid body, this ellipsoid is the inertia ellipsoid associated with the inertia tensor, $\boldsymbol{I}_i$. Asada[17] extended the inertia ellipsoid to multi-rigid body, resulting in GIE associated with the generalized inertia tensor.

The inertia tensor along the GIE principal axes, which are aligned with the Eigenvectors of $\boldsymbol{G}$, is diagonal. The length of each principal axis is the reciprocal of the square root of the corresponding Eigenvalue. In most cases of jumping robots with articulated joints, the emphasis is focused on the whole performance, that is the jumping height and distance, so the dynamics of the robot COM in the operation space is to be investigated.

According to Eq. (4), the generalized inertia tensor can be obtained, as well as its Eigenvalues and Eigenvectors, thus the GIE whose center is the COM of the robot can be shown. Note that here the GIE is a planar ellipse (shown in Fig. 3) because the jumping motion of the robot is in the sagittal plane. Different from the inertia ellipsoid of a single rigid body, the GIE varies its shape depending on location in the operation space. The global characteristics of the robot inertia as a whole can be represented by drawing the GIE at each point in the reachable region or in the jumping trajectory, which is planned.

In Fig. 3, the GIE geometrical shape represents the whole inertia characteristics of the jumping robot COM. The inertia varies with change in the motion direction and space location. If the principal axes have same lengths, that is the GIE is a pure sphere, then the inertia is isotropic. Therefore, the length difference between the major and the minor axes describes the inertia anisotropy. With the extension of robot joints, the GIE varies its shape. When each joint extends to its limit positions, the shape of the GIE becomes long and narrow, while the shape is changed to thick and round in the position far away from the limit positions, so the inertia is more isotropic in the positions far away from its limits than in the limit positions. When each joint is fully extended, namely all links are connected in a straight line, the robot cannot move in the radical direction, locating in a singular position. When the robot reaches the singular position, that is the dashed line in Fig. 3, the GIE will be thinner and converge to a line. The geometrical shape of the GIE can easily describe the robot's dynamic performance.

3. Nonlinear Analysis of a Jumping Robot Based on GIE

The motion of a jumping robot is highly nonlinear, which is mainly resulted from Coriolis and centrifugal forces. From the view point of GIE, the nonlinear forces can be analyzed.

3.1. Nonlinear forces of a jumping robot

Assume A to be a fixed point in the operation space. If the GIE principal axes at A are used as coordinates to represent robot motion in the vicinity of A, the inertia tensor is diagonal with those axes.[17] Let $\boldsymbol{D}_A$ be the diagonal matrix, whose diagonal elements are the Eigenvalues of $\boldsymbol{G}$, λ_1, λ_2. Defining $\dot{\boldsymbol{x}} = [\dot{x}_1, \dot{x}_2]^{\mathrm{T}}$ as a generalized velocity related to the principal axis, the kinetic energy can be written as

$$E_k = \frac{1}{2}\dot{\boldsymbol{x}}^T D_A \dot{\boldsymbol{x}}. \tag{6}$$

Let $\boldsymbol{Q}$ be the generalized forces, including gravity force. $\boldsymbol{Q}$ acts along the principal axis, thus the Lagrange equation referred to the principal axes is

$$\boldsymbol{Q} - \boldsymbol{D}_A\ddot{\boldsymbol{x}} + F_N\left(\dot{x}; \frac{\partial \boldsymbol{D}_A}{\partial x_i}\right) = \boldsymbol{0}, \tag{7}$$

where the second term is the inertia forces, among which there are no interactions along the principal axes, and the third term represents the forces caused by the change of

https://doi.org/10.1017/S0263574712000045 Published online by Cambridge University Press

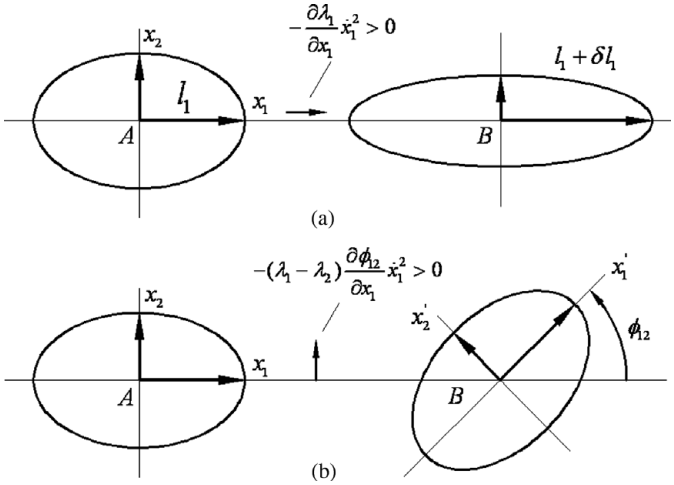


Fig. 4. Change of GIE shape.

inertia tensor. $\boldsymbol{F}_N$ is expressed as

$$\boldsymbol{F}_N = \frac{1}{2}\left[\dot{\boldsymbol{x}}^{\mathrm{T}}\frac{\partial \boldsymbol{D}_A}{\partial x_1}\dot{\boldsymbol{x}}, \dot{\boldsymbol{x}}^{\mathrm{T}}\frac{\partial \boldsymbol{D}_A}{\partial x_2}\dot{\boldsymbol{x}}\right]^{\mathrm{T}} - \left(\frac{\partial \boldsymbol{D}_A}{\partial x_1}\dot{x}_1 + \frac{\partial \boldsymbol{D}_A}{\partial x_2}\dot{x}_2\right)\dot{\boldsymbol{x}}. \tag{8}$$

It can be seen from Eq. (8) that $\boldsymbol{F}_N$ is a nonlinear force because it consists of forces that are proportional to the products of velocities.

3.2. Geometrical description of GIE shape

It can be known from Eq. (8) that the change of inertia tensor will generate nonlinear forces, so the nonlinear characteristics can be analyzed by studying the GIE shape. In Fig. 4, when the robot COM is moved from A to B, the GIE shape will change.

Referred to the principal axes at A, let $\boldsymbol{G}_B$ be the inertia tensor of GIE at B. $\boldsymbol{G}_B$ is then standardized to a diagonal matrix, $\boldsymbol{D}_B$,

$$\boldsymbol{G}_B = \boldsymbol{C}\boldsymbol{D}_B\boldsymbol{C}^{\mathrm{T}}, \tag{9}$$

where $\boldsymbol{C}$ is a standard orthonormal matrix, and the diagonal components of $\boldsymbol{D}_B$ are the Eigenvalues of $\boldsymbol{G}_B$. It corresponds to the lengths of principal axes and determines the GIE shape. $\boldsymbol{C}$ stands for GIE rotation and determines the GIE orientation, so that change of the GIE can be divided into two parts: ① the shape change described by the change in lengths along principal axes; ② the orientation change described by rotation angles about the principal axes.

Assuming that the principal axes have slight change in lengths from l_i to $l_i + \delta l_i$, $i = 1, 2$, as shown in Fig. 4(a), $\boldsymbol{D}_B$ becomes

$$\boldsymbol{D}_B = \mathrm{diag}[\lambda_i + \delta\lambda_i] = \mathrm{diag}\left[\frac{1}{(l_i + \delta l_i)^2}\right]. \tag{10a}$$

Taking Taylor series expansion for $1/(l_i + \delta l_i)^2$ in Eq. (10a) yields

$$\frac{1}{(l_i + \delta l_i)^2} = \frac{1}{l_i^2} - \frac{2}{l_i^3}\delta l_i + \frac{3}{l_i^4}\delta l^2 + \mathbf{O}(\delta l^3),$$

where $\mathbf{O}(\delta l^3)$ denotes the higher order components. Neglecting its second order and higher order, and substituting it into Eq. (10a) gives

$$\boldsymbol{D}_B = \mathrm{diag}[\lambda_i + \delta\lambda_i] = \mathrm{diag}\left[\frac{1}{l_i^2} - \frac{2}{l_i^3}\delta l_i\right]. \tag{10b}$$

$\boldsymbol{C}$ represents the rotation of GIE from A to B. Let $\delta\phi_{ij}$ be a slight rotation in the plane, including $\boldsymbol{x}_i$ (the ith principal axis) and x_j (the jth principal axis).$\delta\phi_{ij}$ is measured from x_i to x_j. Then the orthonormal matrix $\boldsymbol{C}$ can be written as

$$\boldsymbol{C} = \begin{bmatrix} 1 & -\delta\phi_{12} \\ \delta\phi_{12} & 1 \end{bmatrix}. \tag{11}$$

Substituting Eqs. (10b) and (11) into Eq. (9) yields

$$\begin{aligned}\boldsymbol{G}_B &= \begin{bmatrix} 1 & -\delta\phi_{12} \\ \delta\phi_{12} & 1 \end{bmatrix}\begin{bmatrix} \lambda_1 + \delta\lambda_1 & 0 \\ 0 & \lambda_2 + \delta\lambda_2 \end{bmatrix}\begin{bmatrix} 1 & \delta\phi_{12} \\ -\delta\phi_{12} & 1 \end{bmatrix} \\ &= \begin{bmatrix} \lambda_1 + \delta\lambda_1 & -\delta\phi_{12}\lambda_2 + \delta\lambda_2 \\ \delta\phi_{12}\lambda_2 + \delta\lambda_2 & \lambda_2 + \delta\lambda_2 \end{bmatrix}\begin{bmatrix} 1 & \delta\phi_{12} \\ -\delta\phi_{12} & 1 \end{bmatrix} \\ &= \begin{bmatrix} \lambda_1 + \delta\lambda_1 & (\lambda_1 - \lambda_2)\delta\phi_{12} \\ (\lambda_1 - \lambda_2)\delta\phi_{12} & \lambda_2 + \delta\lambda_2 \end{bmatrix}. \end{aligned} \tag{12}$$

Change of inertia tensor, $\delta\boldsymbol{D}_A = \boldsymbol{G}_B - \boldsymbol{D}_A$, is

$$\begin{aligned}\delta\boldsymbol{D}_A &= \begin{bmatrix} \lambda_1 + \delta\lambda_1 & (\lambda_1 - \lambda_2)\delta\phi_{12} \\ (\lambda_1 - \lambda_2)\delta\phi_{12} & \lambda_2 + \delta\lambda_2 \end{bmatrix} - \begin{bmatrix} \lambda_1 & 0 \\ 0 & \lambda_2 \end{bmatrix} \\ &= \begin{bmatrix} \delta\lambda_1 & (\lambda_1 - \lambda_2)\delta\phi_{12} \\ (\lambda_1 - \lambda_2)\delta\phi_{12} & \delta\lambda_2 \end{bmatrix}. \end{aligned} \tag{13}$$

3.3. Nonlinear force analysis of a jumping robot

When a jumping robot moves along the ith principal axis, in the case of the first principal axis, the velocity vector is $\dot{\boldsymbol{x}} = [\dot{x}_1, 0]^T$. This motion will cause nonlinear force. Inserting Eq. (13) into Eq. (8) results in

$$\boldsymbol{F}_N\Big|_{\dot{x}=\begin{bmatrix}\dot{x}_1 \\ 0\end{bmatrix}} = \begin{bmatrix} -\frac{1}{2}\frac{\partial \lambda_1}{\partial x_1} \\ \frac{1}{2}\frac{\partial \lambda_1}{\partial x_2} - (\lambda_2 - \lambda_1)\frac{\partial \phi_{21}}{\partial x_1} \end{bmatrix}\dot{x}_1^2. \tag{14}$$

where $\partial\phi_{21}/\partial x_1$ is the curvature of a curve along which the first principal axis changes its direction, $\partial\lambda_1/\partial x_1$ stands for the change of GIE in the length of the first principal axis.

From the first term in Eq. (14), when the robot moves in the direction of the first principal axis along which the axis length becomes longer, a nonlinear force, $-\dot{x}_1^2 \cdot (\partial\lambda_1/\partial x_1)/2$, will be generated in the same direction, and acts on the robot. It can be known from the second term that when the length of the first axis varies along the second axis, a nonlinear force, $-\dot{x}_1^2 \cdot (\partial\lambda_1/\partial x_2)/2$, acts in the direction of the second axis. In addition, if GIE rotates in the plane of $x_1 - x_2$, a nonlinear force,$-(\lambda_1 - \lambda_2)(\partial\phi_{12}/\partial x_1)\dot{x}_1^2$, acts along the second axis. The nonlinear force caused by the change of GIE is proportional to differences in Eigenvalues, so if GIE is isotropic, these nonlinear forces will not occur.

https://doi.org/10.1017/S0263574712000045 Published online by Cambridge University Press

The nonlinear forces are shown in Fig. 4. In Fig. 4(a), when the robot moves along a major axis, which increases in its length, means that $-\partial\lambda_1/\partial x_1 > 0$. A positive force, $-(\partial\lambda_1/\partial x_1)\dot{x}_1^2/2$, acts along the major axis. In Fig. 4(b), the GIE rotates in the counterclockwise direction in the plane of $x_1 - x_2$, where the length of x_1 axis is longer than that of x_2 axis. Thus, a positive force, $-(\lambda_1 - \lambda_2)(\partial\phi_{12}/\partial x_1)\dot{x}_1^2$, acts along x_2 axis.

4. GIE-Based Optimization Design of a Jumping Robot

The GIE shape in the Cartesian coordinates can describe the global characteristics of robot dynamics as a whole. Since the geometric shape of the GIE can express inertia effects and nonlinear characteristics, the GIE can be used in the design of a jumping robot, providing a base for the robot mechanism design.[19] The dynamic performance of a jumping robot can be improved by increasing the isotropy of the GIE in the reachable region.

The inertia characteristics can be an index to measure the jumping robot's performance. The target is to minimize the inertia and obtain isotropic inertia. The limit value can be computed by transforming the index into mathematical expression to achieve the optimization of the robot design. Furthermore, according to the GIE shape, the workspace region of the robot can be reasonably determined.

4.1. Optimization of mechanism parameters

The generalized inertia of a robot includes configuration parameters and mechanism parameters. The former are state variables, while the latter are design variables. Therefore, the generalized inertia index depends on state variables, varying with change of robot configuration. In other words, the measuring index has different values at different points in the robot operation space.[20,21] To measure the whole dynamic performance during the jumping motion of a robot and to globally optimize, the objective function is selected as

$$\boldsymbol{F}(\boldsymbol{\chi}) = \frac{\int_{\boldsymbol{D}_\theta} f(\theta, \boldsymbol{\chi}) d\boldsymbol{D}_\theta}{\int_{\boldsymbol{D}_\theta} d\boldsymbol{D}_\theta}, \tag{15}$$

where $f(\boldsymbol{\theta}, \boldsymbol{\chi}) = k(\boldsymbol{G})$. $k(\boldsymbol{G})$ is the condition number of the matrix, $\boldsymbol{G}$, and $\boldsymbol{D}_\theta$ is the joint space of the jumping robot.

Optimizing Eq. (15) as an objective function will be time-consuming because of complex computation. To simplify optimization, discrete points of a jumping trajectory are adopted. To obtain the isotropy, the objective function is changed into square function to avoid complexity of integral computation. During optimization, the mechanism parameters are constrained within a specified region. Using 500 discrete points, based on GIE, the mathematical model of the jumping mechanism parameter optimization is

$$\begin{aligned}
&\min\ F(l_i, a_i, m_i) = \sum_{i=1}^{500} (k_{i+1}(G) - k_i(G))^2, \\
&\text{s.t.}\ \ m = \sum_{i=1}^{4} m_i = 2.85 \text{ kg}, \\
&\quad l = \sum_{i=1}^{4} l_i = 0.7125 \text{ m}, \\
&\quad 0 \le a_i \le 1,\ i = 1,\ 2,\ 3,\ 4 \\
&\quad 0.0652 \text{ m} \le l_1 \le 0.1625 \text{ m}, 0.1 \text{ m} \le l_2,\ l_3 \le 0.2 \text{ m}, \\
&\quad 0.25 \text{ m} \le l_4 \le 0.35 \text{ m}, \\
&\quad 0.35 \text{ kg} \le m_1 \le 0.55 \text{ kg}, 0.5 \text{ kg} \le m_2, m_3 \le 0.7 \text{ kg}, \\
&\quad 1.1 \text{ kg} \le m_4 \le 1.3 \text{ kg},
\end{aligned} \tag{16}$$

where $k_{501}(\boldsymbol{G}) = k_1(\boldsymbol{G})$.

Table I. Mechanism parameter optimization results of a jumping leg robot based on GIE.

	Initial design	GIE-based optimization design
a_1	0.5	0.17
a_2	0.5	0.71
a_3	0.5	0.13
a_4	0.5	0.82
m_1/kg	0.45	0.438
m_2/kg	0.6	0.588
m_3/kg	0.6	0.59
m_4/kg	1.2	1.234
l_1/m	0.1125	0.075
l_2/m	0.15	0.177
l_3/m	0.15	0.141
l_4/m	0.3	0.319
Objective function value	0.2493	1.1 e-6

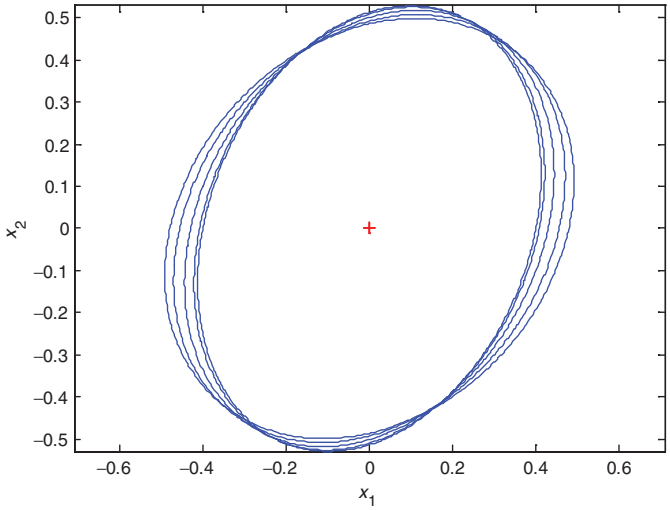


Fig. 5. (Colour online) GIE of initial design.

The optimization results are shown in Table I. Figures 5 and 6 show the GIE of a jumping robot in the ground phase. It can be seen from comparison between Fig. 5 and Fig. 6 that the GIE shape is closer to a circle after the mechanism parameters are optimized. This means that the GIE isotropy

https://doi.org/10.1017/S0263574712000045 Published online by Cambridge University Press

Table II. Optimization results for isotropic configuration.

Joint	Initial angle	Optimized angle
θ_1	165°	90°
θ_2	−150°	−56.3°
θ_3	150°	102.6°
θ_4	−150°	−91.9°

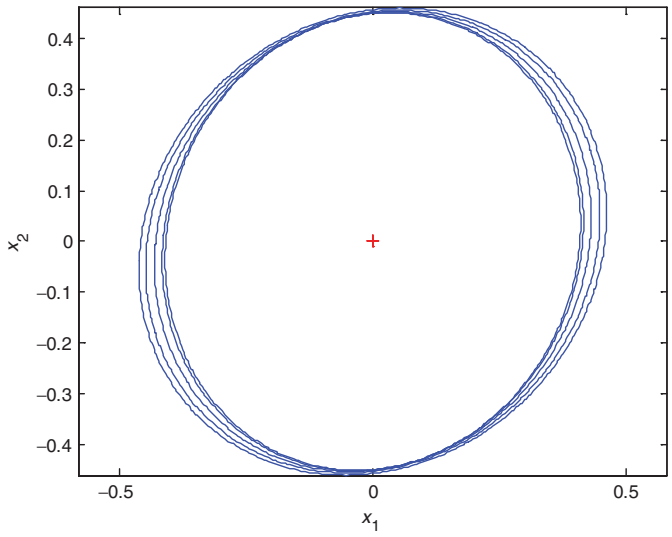


Fig. 6. (Colour online) GIE with optimization parameters.

is increased, and the GIE change extents in both axis lengths and orientation are all reduced, so the nonlinear forces are also reduced during the robot motion, making the robot easy to control. Thus, the optimization of the jumping robot mechanism parameters is validated.

4.2. Isotropic configuration of a jumping robot based on GIE

The isotropic joint configuration computed from the condition that the mechanism parameters are all known can be applied to the robot trajectory planning to improve dynamic performance in terms of motion planning.[21] For simple computation, the condition number is still selected as the objective function for optimization. To avoid singular configuration, each joint angle is restricted. The mathematical model for optimization to obtain the isotropic configuration is

$$\begin{aligned} &\min\ f(\boldsymbol{\theta}) = k(\boldsymbol{G}) \\ &\text{s.t.}\ \ 15^\circ < \theta_1, \theta_3 < 165^\circ \\ &\qquad -165^\circ < \theta_2, \theta_4 < -15^\circ \end{aligned}, \tag{17}$$

where the parameters of matrix $\boldsymbol{G}$ are the initial design parameters as shown in Table I.

The optimization results are shown in Table II. The configuration of the mechanism model with optimized joint parameters is shown in Fig. 7, and the corresponding GIE is shown in Fig. 8, from which it is observed that the GIE shape is nearly a pure circle, demonstrating that the optimized joint angles make the robot mechanism isotropic and little nonlinear forces caused by the change of GIE orientation.

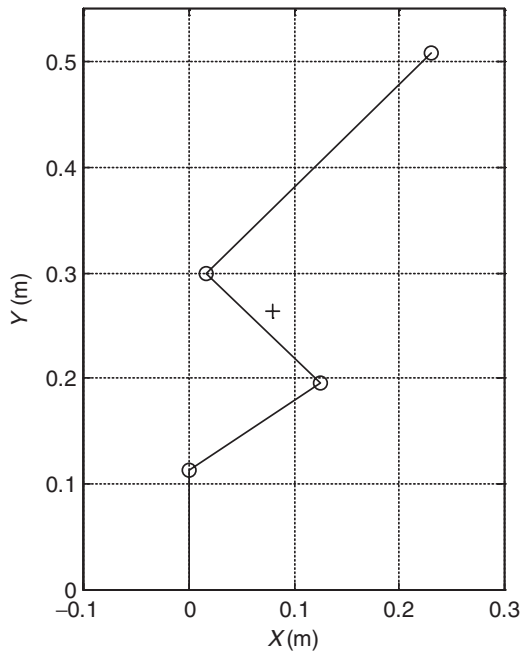


Fig. 7. Isotropic configuration of the mechanism model.

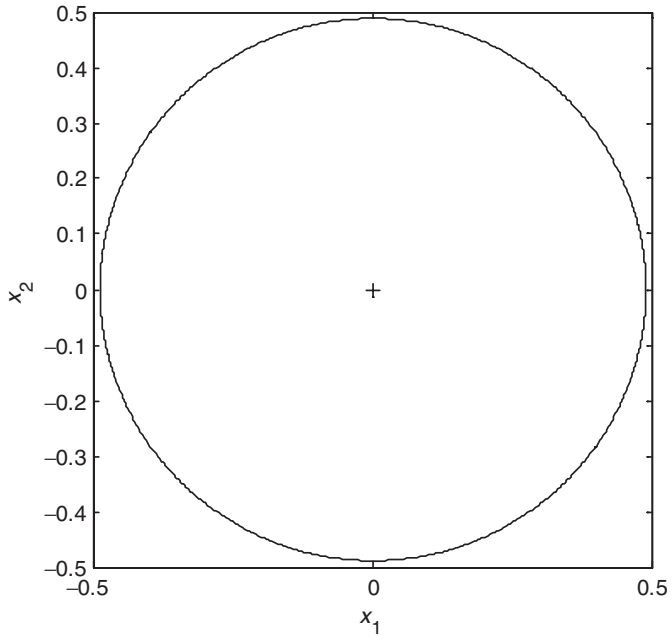


Fig. 8. Isotropic GIE.

5. Conclusions

The dynamic performance of the takeoff phase has great influence on the robot jumping height and distance. The GIE method used on manipulators is applied here to analyze the robot dynamic performance in the operation space. From the kinetic energy of the mechanism, the generalized inertia tensor and GIE of the robot are obtained. Analyzing the GIE shape, the dynamics of the robot has the following characteristics:

1. In some joint configurations, a large difference in axis lengths between the major and minor axes shows that the

https://doi.org/10.1017/S0263574712000045 Published online by Cambridge University Press

generalized inertia of the robot COM varies significantly depending on the motion direction.
2. In some joint configurations, changes in the GIE shape and orientation are very large, the robot dynamics then involves large nonlinear forces.
3. When the jumping robot moves closely to the singular configuration, the GIE shape becomes long and narrow. This means that the generalized inertia of the robot COM is very large along the minor axis of the GIE. In the case of same kinetic energy, the velocity of the robot COM along the direction is very small, while the generalized inertia of the robot COM is very small along the major axis of the GIE along which the velocity is also very large. When the robot moves from non-singular configuration to singular configuration, the GIE shape varies significantly, causing large nonlinear forces and unbalanced inertia characteristics, degrading the robot dynamic performance and precise motion.

The GIE shape can describe inertia effects and nonlinear characteristics, so inertia characteristics can be an index to evaluate the robot performance to optimize its design such that minimum and isotropic inertia characteristics are achieved. After the optimization of a jumping robot, the GIE shape tends to be a pure circle with optimized structure parameters, and the robot mechanism is isotropic with the optimized joint angles, leading to no nonlinear forces caused by change of GIE in the robot mechanism and improving the robot control performance.

It should be pointed out that the task of this paper is to optimize the mechanism parameters. As this task is finished in the design phase, there is no strict real-time requirement. The optimization is simplified to reduce the consuming time, and we adopt simple objective function. What is more, discrete points of the jumping trajectory are also adopted to simplify the optimization. Though current computers generally have high operational performance and fast computation speed, the consuming time will increase as the discrete point is increased. This may slow the design process, and too many discrete points cannot contribute to improve the optimization design results to a large extent, so in practical application one should not select too many discrete points for optimization.

References

1. A. H. Ji, Z. D. Dai and L. S. Zhou, "Research development of bio-inspired robotics," *Robot* **27**(3), 284–288 (2005).
2. C. Yong, "Jumping Robot Based on the Kinematics Performance of Locust," **In**: *Proceedings of the 2nd International Conference on Industrial Mechatronics and Automation (ICIMA)*, Wuhan, China (May. 30–31, 2010) pp. 33–36.
3. M. Kovac, M. Schlegel, J. C. Zufferey and D. Floreano, "A Miniature Jumping Robot with Self-Recovery Capabilities," **In**: *Proceeding s of IEEE/RSJ International Conference on Intelligent Robots and Systems (IROS)*, St. Louis, MO, USA (Oct. 11–15, 2009) pp. 583–588.
4. D. H. Kim, J. H. Lee, I. Kim, S. H. Noh and S. K. Oho, "Mechanism, control, and visual management of a jumping robot," *Mechatronics* **18**(10), 591–600 (2008).
5. M. Kovac, M. Fuchs, A. Guignard, J. C. Zufferey and D. Floreano, "A Miniature 7G Jumping Robot," **In**: *Proceedings of IEEE International Conference on Robotics and Automation (ICRA)*, Pasadena, CA, USA (May 19–23, 2008) pp. 373–378.
6. M. Yamakita,Y. Omagari and Y. Taniguchi, "Jumping cat robot with kicking a wall," *J. Robot. Soc. Japan* **26**(3), 934–938 (1994).
7. K. Arikawa and T. Mita, "Design of Multi-DOF Jumping Robot," **In**: *Proceedings of IEEE International Conference on Robotics and Automation (ICRA)*, Washington, DC, USA (May 11–15, 2002) pp. 3992–3997.
8. S. H. Hyon, N. Yokoyama and E. Takashi, "Back Handspring Robot-Target Dynamics-Based Control," **In**: *Proceedings of 2004 IEEE/RSJ International Conference on Intelligent Robots and Systems (IROS)*, Sendai, Japan (Sep. 28–Oct. 2, 2004) pp. 248–253.
9. C. B. Matthew, D. Q. Roger, H. Geon, S. M. Phillips, B. Drennan, A. Fife, H. Verma and R. D. Beer, "Design of a Cricket Microrobot," **In**: *Proceedings of the 2000 IEEE International Conference on Robotics & Automation (ICRA)*, San Francisco, CA, USA (Apr. 24–28, 2000) pp. 1109–1114.
10. S. Laksanacharoen, A. J. Pollack, G. M. Nelson, R. D. Quinn and R. E. Ritzmann, "Biomechanics and Simulation of Cricket for Microrobot Design," **In**: *Proceedings of the IEEE International Conference on Robotics and Automation (ICRA)*, San Francisco, CA, USA (Apr. 24–28, 2000) pp. 1088–1094.
11. S. H. Hyon and T. Mita, "Development of a Biologically Inspired Hopping Robot-'Kenken,"' **In**: *Proceedings of the 2002 IEEE International Conference on Robotics Automation (ICRA)*, Washington, DC, USA (May 11–15, 2002) pp. 3984–3991.
12. R. Niiyama, A. Nagakubo and Y. Kuniyoshi, "A Bipedal Jumping and Landing Robot with an Artificial Musculoskeletal System," In: *Proceedings of the IEEE International Conference on Robotics and Automation (ICRA)*, Rome, Italy (Apr. 10–14, 2007) pp. 2546–2551.
13. H. C. Wong and D. E. Orin, "Dynamic Control of a Quadruped Standing Jump," **In**: *Proceedings of the IEEE International Conference on Robotics and Automation (ICRA)*, Atlanta, GA, USA (May 2–6, 1993) pp. 346–351.
14. Y. P. Yang, T. Geng and Y. Guo, "Structure and trajectory planning of a novel flipping robot," *J. Shanghai Jiaotong Univ.* **7**(7), 1110–1113 (2003).
15. G. P. He, X. L. Tan and X. H. Zhang, "Vertical hopping control of elastic one-legged Robot with two actuated arms," *Chin. J. Mech. Eng.* **43**(5), 44–49 (2007).
16. L. E. Ma, W. J. Ge and Z. B. Huang, "Positive kinematics analysis on bionic kangaroo-hopping robot," *J. Mach. Des.* **22**(3), 28–30 (2005).
17. H. Asada, "A geometrical representation of manipulator dynamics and its application to arm design," *J. Dyn. Syst. Meas. Control* **9**(105), 131–142 (1983).
18. Z. H. Xu, T. S. Lv, X. Y. Wang and J. Liu, "Motion optimization for jumping robot based on inertia matching manipulability," *J. Shanghai Jiaotong Univ.* **42**(7), 1154–1158 (2008).
19. R. V. Mayorga, J. Carrera and M. M. Oritz, "A kinematics performance index based on the rate of change of a standard isotropy condition for robot design optimization," *Robot. Auton. Syst.* **53**, 153–163 (2005).
20. O. Khatib and A. Bowling, "Optimization of the Inertial and Acceleration Characteristics of Manipulators," **In**: *Proceedings of the IEEE International Conference on Robotics and Automation (ICRA)*, Minneapolis, MN, USA (Apr. 22–28, 1996) pp. 2883–2889.
21. O. Khatib and J. Burdick, "Optimization of dynamics in manipulator design: The operational space formulation," *Int. J. Robot. Autom.* **2**(2), 90–98 (1987).

https://doi.org/10.1017/S0263574712000045 Published online by Cambridge University Press